Chaos, Solitons and Fractals 202 (2026) 117611

Contents lists available at ScienceDirect

Chaos, Solitons and Fractals

journal homepage: www.elsevier.com/locate/chaos

Estimation of the parameters of q-Gaussian distributions in the standard map

Zulkarnain [a,b], H. Susanto [c], C.G. Antonopoulos [a,*]

[a] School of Mathematics, Statistics and Actuarial Science, University of Essex, Wivenhoe Park, Colchester, CO4 3SQ, United Kingdom
[b] Department of Mathematics, Faculty of Mathematics and Natural Sciences, Universitas Riau, Pekanbaru, 28293, Indonesia
[c] Department of Mathematics, Khalifa University, Abu Dhabi, PO Box 127788, United Arab Emirates

ARTICLE INFO

MSC:
37N05
37M05
82C70
65K10
90C59

Keywords:
Standard map
q-Gaussian distribution
Non-extensive statistical mechanics
Multi-objective optimization
Genetic algorithm
Integrable dynamics
Asymptotic scaling

ABSTRACT

We present a novel methodology for estimating the parameters of the q-Gaussian distribution within the framework of non-extensive statistical mechanics, applied to the standard map (Chirikov-Taylor map) across its chaotic, regular, and integrable regimes. Our approach combines a genetic algorithm with multi-objective optimization, simultaneously minimizing the discrepancy between the numerical probability density function (PDF) and the q-Gaussian while enforcing normalization to unit area. This framework yields highly accurate parameter estimates, revealing optimal q and b values that provide an exceptional fit to the numerical PDFs. Notably, the estimated q values differ from previous reports, highlighting the sensitivity of parameter inference to fitting methodology. For the integrable case ($K = 0$), we uncover a striking asymptotic scaling law: q approaches its theoretical value of 2 extremely slowly with iteration number, following a power-law trend that implies an extraordinarily large number of iterations are required for convergence. Overall, our results demonstrate that the proposed method robustly captures the statistical properties of the standard map across different dynamical regimes and suggest its potential for broader applications to other deterministic dynamical systems, offering new insights into the emergence of non-extensive statistical behavior.

1. Introduction

The standard map, introduced by Chirikov in 1979 (also known as the Chirikov-Taylor map), is one of the most widely studied models in nonlinear dynamics and chaos theory due to its simple structure yet complex behavior in both regular and chaotic regimes [1]. It serves as a fundamental tool for exploring the dynamics of Hamiltonian systems and offers insights into the transition from order to chaos. Depending on the nonlinearity parameter, the phase space of the standard map typically consists of a mixture of regular, quasi-periodic and chaotic regions, making it an ideal candidate for studying statistical mechanics in systems with non-trivial dynamics [2]. To capture the statistical properties of such systems, especially when dealing with non-extensive statistics, the q-Gaussian distribution was shown to be particularly effective [3–5].

The q-Gaussian function, derived from Tsallis's non-extensive statistical mechanics [6], is a generalization of the standard Gaussian distribution. It is frequently employed to model systems where power-law tails or deviations from Boltzmann–Gibbs statistics are observed. Fitting the probability density function (PDF) derived from the dynamics to the q-Gaussian allows one to analyze and quantify the statistical behavior of both regular and chaotic regions.

* Corresponding author.
E-mail address: canton@essex.ac.uk (C.G. Antonopoulos).

https://doi.org/10.1016/j.chaos.2025.117611
Received 3 June 2025; Received in revised form 6 November 2025; Accepted 11 November 2025
Available online 20 November 2025

In statistical mechanics, the characterization of the dynamics of both low- and high-dimensional systems is often based on analyzing the distributions of statistical variables (probes) derived from their trajectories. In chaotic systems, the PDFs of these variables typically converge to a Gaussian distribution, signifying chaotic behavior. However, some systems exhibit PDFs that can be approximated by q-Gaussian distributions within the framework of non-extensive statistical mechanics [3], which are associated with weakly chaotic dynamics [7–11].

For the standard map [12–15], previous studies [5,16] have demonstrated that the PDF of the system depends significantly on the location of the initial conditions. When the initial conditions are placed in the chaotic sea, characterized by a positive Lyapunov exponent [17], the resulting distribution is well approximated by a Gaussian. More broadly, the authors in [5] observed that the numerical PDFs in the case of the standard map take the form of either a Gaussian, a q-Gaussian, or a mixed-type distribution that is a linear combination of both. In particular, the authors in [5,16] reported that when the initial conditions lie within islands of stability, including the non-integrable and integrable cases of the map, the distribution converges to a q-Gaussian with $q = 1.935$, without discussing the method used to estimate it numerically. Moreover, the authors in [18] reported that $q = 2$ in the integrable case of the map, employing theoretical arguments, without presenting any numerical evidence. This discrepancy in the q values in the case of regular dynamics, and lack of introduction of any algorithmic approach to compute the q-Gaussian parameters, including q, motivated us to develop here an algorithmic approach to reliably estimate the q-Gaussian parameters, including the q entropic index.

In our study of the integrable case ($K = 0$) of the standard map, we observed a striking asymptotic behavior in the estimated q values. By systematically increasing the number of iterations, we found that q gradually approaches the theoretical limit of 2, following a slow power-law scaling, $q(N) \sim a\, N^b$, with a very small negative exponent b. This demonstrates that convergence to $q = 2$ requires an extraordinarily large number of iterations, highlighting that even in the integrable regime, the approach to the theoretical q-Gaussian is exceptionally slow. Our results underscore the importance of accounting for asymptotic scaling effects when interpreting numerical estimates of q, particularly in systems exhibiting regular dynamics. Fig. 9 illustrates this behavior by showing the estimated q as a function of $1/N$, with a power-law fit capturing the slow convergence toward the theoretical limit.

Hence it is of paramount importance to determine the optimal parameters of the q-Gaussian that accurately fit the numerical PDF, particularly in complex, mixed dynamics such as those of the standard map, as this still remains a challenge [19]. In particular, fitting probability distribution functions with the q-Gaussian function is challenging due to its nonlinear dependence on the shape parameter q, which significantly affects the distribution's tails and makes optimization sensitive and potentially unstable. The absence of a closed-form normalization constant for general q values complicates likelihood-based methods, often requiring numerical integration. Moreover, the q-Gaussian can exhibit compact support for $q < 1$ or heavy power-law tails for $q > 1$, demanding large datasets to fit accurately. Parameter interdependence and the lack of standardized tools further add to the difficulty, making fitting susceptible to overfitting and poor convergence without careful handling.

This paper aims to address this challenge by developing a novel procedure to determine the parameters of the q-Gaussian function for the numerical PDF, and we apply it to the case of the standard map. By employing a multi-objective optimization approach using a genetic algorithm, we aim to achieve a well-fitted representation of the statistical properties of the system. Genetic algorithms have proven effective for optimization problems in nonlinear and chaotic systems due to their ability to search large parameter spaces and avoid local minima [20]. The approach outlined in this paper provides an efficient and reliable method for modeling the statistical behavior of the standard map, enhancing our understanding of the underlying dynamics in both regular and chaotic regimes.

The paper is organized as follows: Section 2 provides an overview of the dynamics of the standard map, while Section 3 introduces the Gaussian and q-Gaussian distributions. In Section 4, we present a detailed explanation of the PDFs of the standard map's trajectories, along with the methodology used to generate them. Section 5 describes the fitting technique applied to the data. Our findings are presented in Section 6, and finally, we summarize our work in the Conclusions section.

2. Dynamics of the standard map

We consider the standard map [12–15], defined by

$$\begin{aligned} p_{i+1} &= p_i - K \sin x_i, \\ x_{i+1} &= x_i + p_{i+1}, \end{aligned} \tag{1}$$

where $i \geq 0$ is the iteration index, and p_i, x_i are taken modulo 2π. Here, $K \geq 0$ is the nonlinearity parameter. For $K = 0$, the map is linear and integrable, admitting only periodic and quasi-periodic trajectories. In the phase space (x_i, p_i), quasi-periodic trajectories lie on invariant curves that form islands of stability around stable periodic orbits, as shown in panel (a) of Fig. 1. The nature of the observed trajectory depends on the initial condition (x_0, p_0) and K. We plot trajectories in different colors in Fig. 1 to appreciate the rich dynamics exhibited by the standard map (1).

As we can see in Fig. 1(a), for small values of $K > 0$, the system exhibits predominantly regular, quasi-periodic behavior, where trajectories form closed invariant curves in phase space, and the system remains nearly integrable. These trajectories are stable, and the system evolves in a predictable manner. However, as K increases, the standard map (1) begins to exhibit chaotic behavior, illustrated in black in panels (b), (c), and (d) in Fig. 1 for $K = 0.2$, 0.6, and 2, respectively. The phase spaces of the map for four representative values of $K > 0$ (namely, $K = 0.2$, 0.6, 2, and 10) are shown in panels (a)–(d) in Fig. 1. Black regions correspond to areas in phase space occupied by chaotic trajectories, which become increasingly dominant as K increases.

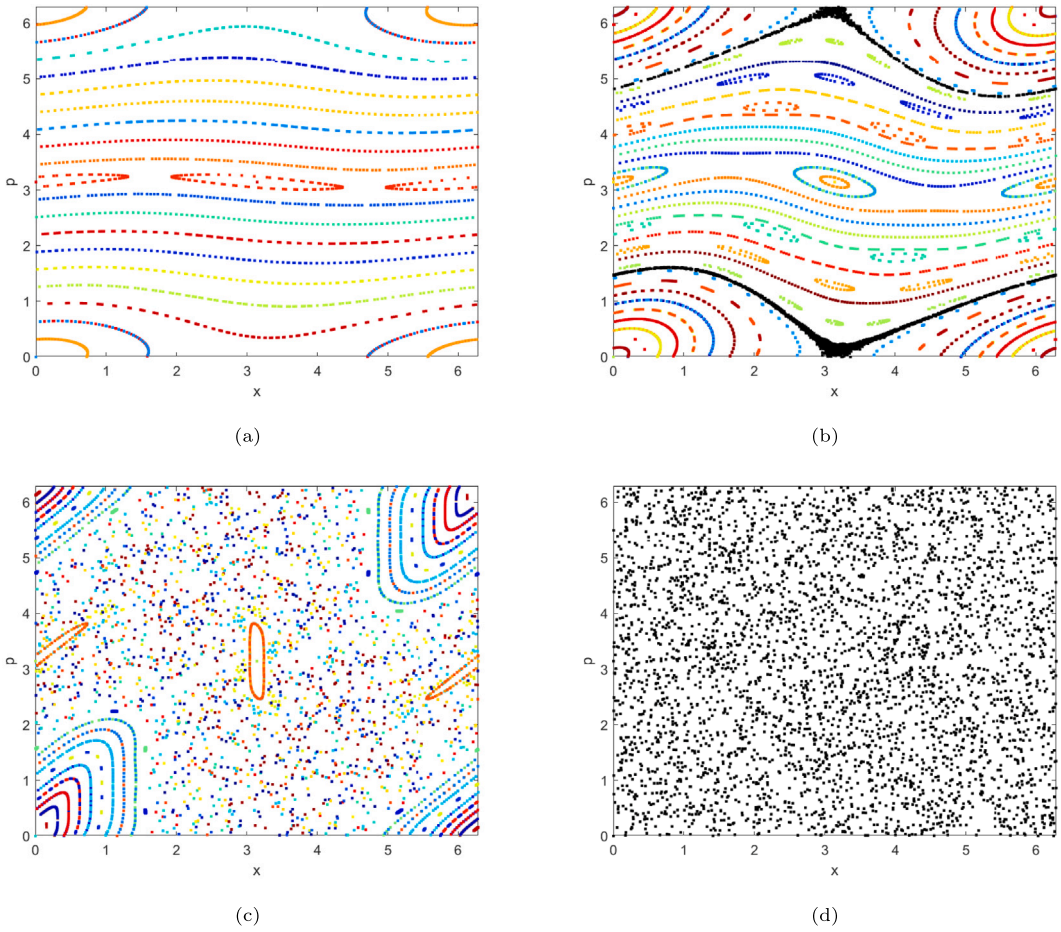

Fig. 1. Phase portraits (x, p) of the standard map (1) for (a) $K = 0.2$, (b) $K = 0.6$, (c) $K = 2$, and (d) $K = 10$. As K increases, chaotic behavior becomes increasingly dominant. Different colors indicate trajectories originating from different initial conditions. In panels (b), (c), and (d), black points and regions correspond to chaotic trajectories, while colored points indicate regular dynamics.

Fig. 2 shows the corresponding plots of the maximum Lyapunov exponent (mLE), computed following [17]. In these plots, black indicates regular motion, while other colors denote weakly or strongly chaotic behavior, represented by positive values on the color scale. These results corroborate those in Fig. 1, clearly demonstrating that as K increases, the proportion of chaotic regions in the phase space $[0, 2\pi]\times[0, 2\pi]$ grows. As it can be seen in panel (d) for $K = 10$, there are no visible islands of stability; chaos dominates the entire phase space, with the maximum Lyapunov exponent reaching approximately 1.8, the maximum value shown on the color bar.

The authors in [5] show that the dynamics of the standard map (1), which is area-preserving and conservative, exhibit a transition from Boltzmann–Gibbs to Tsallis statistics as the parameter K decreases toward zero. Their results clearly delineate the domains of validity for both Boltzmann–Gibbs and Tsallis statistical frameworks. Interestingly, they found that distributions generated from initial conditions located within the islands of stability of the standard map (1), whether sampled from a single region or multiple such regions, consistently result in a value of $q = 1.935$, independent of the value of K. By contrast, initial conditions sampled from the chaotic sea invariably yield Gaussian distributions.

However, accurately identifying the optimal parameters of the q-Gaussian that best fit the numerical PDF, particularly in complex, mixed dynamical regimes such as those of the standard map (1), remains a challenging problem [19]. This is due to the nonlinear dependence of the q-Gaussian on q, which significantly affects the distribution's tails and makes optimization sensitive and potentially unstable. Also, the absence of a closed-form normalization constant for general q values complicates likelihood-based methods, often requiring numerical integration. Moreover, the q-Gaussian can exhibit compact support for $q < 1$ or heavy power-law tails for $q > 1$, demanding large datasets to fit accurately. Parameter interdependence and the lack of standardized tools further add to the difficulty, making fitting susceptible to overfitting and poor convergence without careful handling.

In this work, we revisit the case where initial conditions are placed within islands of stability and demonstrate that a systematic and precise calculation of the resulting PDF does not reproduce the value $q = 1.935$ reported in [5]. By "systematic and precise",

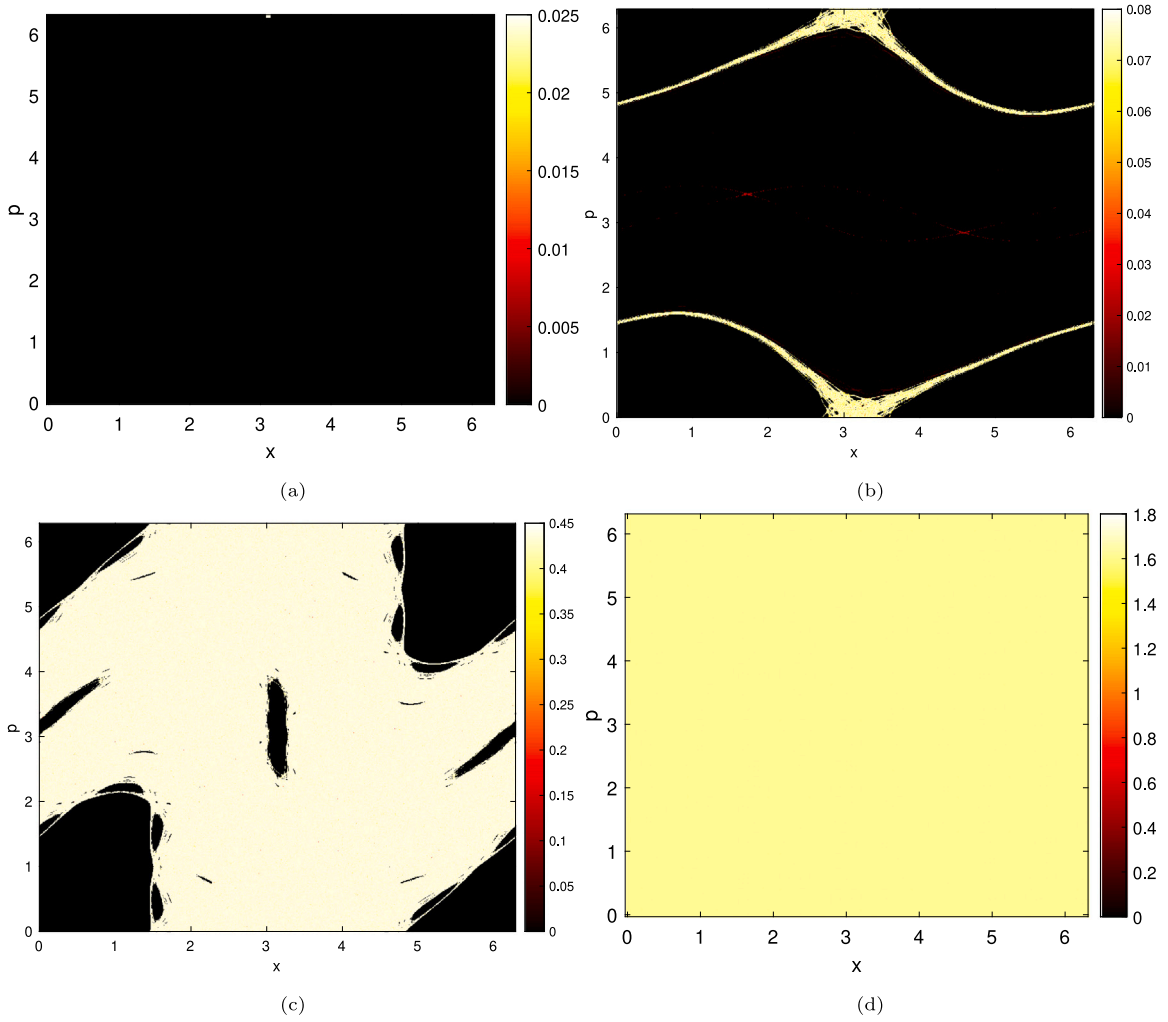

Fig. 2. Phase space (x, p) plots of the mLEs for the standard map (1) at (a) $K = 0.2$, (b) $K = 0.6$, (c) $K = 2$, and (d) $K = 10$. For each value of K, the mLE is computed using 10^6 initial conditions, uniformly distributed over the domain $[0, 2\pi] \times [0, 2\pi]$. Each trajectory is iterated 10^7 times. The color bar indicates the value of the mLE, starting at 0.

we refer to a method that ensures the area under the PDF is numerically very close to 1, and that the fit to the data is as accurate as possible, as quantified by the objective functions defined in Eqs. (11) and (12) here.

To achieve this, we employ a multi-objective optimization approach based on a genetic algorithm, which is described in detail in Section 5. Genetic algorithms have proven effective for optimization problems in nonlinear and chaotic systems due to their ability to explore large parameter spaces and avoid local minima [20]. The method presented in this paper offers an efficient and reliable means of modeling the statistical behavior of the standard map, thereby enhancing our understanding of its underlying dynamics in both regular and chaotic regimes. Our results show that the proposed method can accurately fit the PDFs of both dynamical types, offering deeper insight into the complex behavior of the standard map. We anticipate that this approach will also be effective for other dynamical systems, thereby broadening its applicability.

3. Gaussian and q-Gaussian probability distributions

The Gaussian distribution function is given by

$$G(x) = G(0)e^{-bx^2}, \tag{2}$$

for some (scaling) parameter $b \in \mathbb{R}$, where $G(0)$ is a normalization constant that adjusts the height of the distribution [3]. If we apply the transformation

$$\widetilde{x} = xG(0),$$

$$\widetilde{G}(\widetilde{x}) = G(x)/G(0), \qquad \widetilde{b} = b/G(0)^2, \tag{3}$$

the Gaussian distribution (2) can be rewritten in the form

$$\widetilde{G}(\widetilde{x}) = e^{-\widetilde{b}\widetilde{x}^2}, \tag{4}$$

where $\widetilde{b}$ is a scale constant. This transformation is important because it normalizes the Gaussian distribution so that $\widetilde{G}(0) = 1$. Solving

$$\int_{-\infty}^{\infty} \widetilde{G}(\widetilde{x})\, d\widetilde{x} = 1,$$

which implies that $\widetilde{G}$ is a probability density function, we obtain $\widetilde{b} = \pi$. Therefore, the Gaussian PDF in Eq. (4) is characterized by the parameter value $\widetilde{b} = \pi$.

Following [3], one can also define the q-Gaussian distribution function as

$$G_q(x) = a \exp_q(-b_q x^2),$$

where

$$\exp_q(x) = (1 + (1-q)x)^{1/(1-q)}, \text{ with } (1 + (1-q)x) > 0. \tag{5}$$

Using the same transformation as before (i.e., Eqs. (3)), we define

$$\widetilde{x} = xG_q(0), \qquad \widetilde{G}_q(\widetilde{x}) = G_q(x)/G_q(0),$$

and obtain

$$\widetilde{G}_q(\widetilde{x}) = \exp_q\left(-\widetilde{b}\widetilde{x}^2\right), \tag{6}$$

where $\widetilde{b}$ is a scaling constant, $\widetilde{G}_q(0) = 1$, and $1 \le q \le 3$. Eq. (6) is equivalent to

$$\widetilde{G}_q(\widetilde{x}) = \left(1 - (1-q)\widetilde{b}_q\widetilde{x}^2\right)^{1/(1-q)}, \text{ where } 1 - (1-q)\widetilde{b}_q\widetilde{x}^2 > 0, \tag{7}$$

with $\widetilde{G}_q$ satisfying

$$\int_{-\infty}^{\infty} \widetilde{G}_q(\widetilde{x})\, d\widetilde{x} = 1, \tag{8}$$

implying that $\widetilde{G}_q$ is a valid PDF. We will take Eq. (8) into account in fitting and Eq. 6, where we discuss our proposed method for the accurate numerical computation of the q-entropic index from the PDFs of regular and chaotic dynamics in the standard map.

Within this framework, the distribution (7) converges to the Gaussian distribution (4) in the limit $q \to 1$, which implies that Eq. (7) includes the Gaussian PDF as a special case. The q-exponential (5) plays a central role in generalizing probability distributions and statistical mechanics to non-extensive systems, where classical assumptions such as entropy additivity no longer apply.

4. Numerical computation of the probability density function

Here, we describe the procedure used to compute numerically the PDF of a variable generated by the trajectories of a map, following the methodology outlined in [5]. In our case, the map in question is the standard map, defined by Eq. (1). The resulting numerical PDF will be used in the next section to compute the q-entropic index for regular and chaotic trajectories of the standard map, using a multi-objective optimization approach, specifically, a genetic algorithm.

Following [5], we randomly choose M initial conditions $x_0^{(j)}$ for $j = 1, 2, \ldots, M$. Each initial condition is then iterated for N steps using the equations of the standard map (1). We define the associated random variables X_j by

$$X_j = \sum_{i=1}^{N} \left(x_i^{(j)} - \langle x \rangle\right), \quad j = 1, 2, \ldots, M, \tag{9}$$

where $x_i^{(j)}$ denotes the ith iterate of the jth trajectory, and $\langle x \rangle$ is the average over all M initial conditions and N iterations, given by

$$\langle x \rangle = \frac{1}{MN} \sum_{j=1}^{M} \sum_{i=1}^{N} x_i^{(j)}.$$

To generate the numerical PDFs, we first construct a histogram of the values $\{X_j\}$ and compute the corresponding probability distribution $P(X_j)$ for a given value of K. The results are visualized in Figs. 3(a) - 3(b), where we plot $P(0)X_j$ on the horizontal axis and $P(X_j)/P(0)$ on the vertical axis. This rescaling produces a normalized PDF with unit area, as required by Eq. (8).

In computing the PDFs, it is essential to carefully determine the bin width, as different binning choices can significantly affect the resulting shape of the distribution and the parameters of the q-Gaussian function. For instance, using too few bins may lead to a

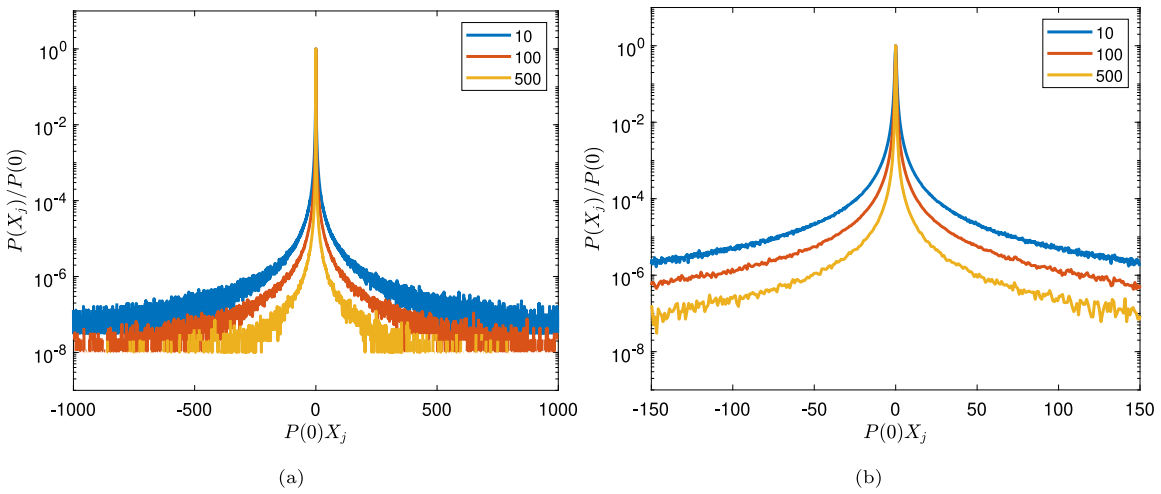

Fig. 3. Panel (a): The normalized PDF of the variable X_j for three different bin widths: 10 (blue curve), 100 (red curve), and 500 (yellow curve). In all cases, $P(0)$ is defined as the height of the central bin corresponding to $P(0)X_j = 0$. Panel (b): A zoomed-in view of the normalized PDF of X_j, similar to that shown in Fig. 3(a), restricted to the interval $[-150, 150]$ on the horizontal axis.

loss of detail, over-smoothing, misleading representations, or increased variance within each bin. Conversely, using too many bins can introduce excessive noise, lead to overfitting, reduce interpretability, overemphasize outliers, and increase computational cost. We address this issue in Section 5 by selecting the optimal PDF according to two key criteria: (a) the PDF must best fit the Gaussian function in the chaotic case and the q-Gaussian function in the regular case, with minimal fitting error; and (b) the PDF must have an area as close as possible to 1, in accordance with Eq. (8).

Fig. 3(a) shows the normalized PDF of X_j computed using 10 (blue curve), 100 (red curve), and 500 (yellow curve) bins. In all cases, $P(0)$ is defined as the height of the central bin, which contains the value 0 on the horizontal axis. In this figure, we consider the integrable case of the map with $K = 0$. We randomly select 10^8 initial conditions and iterate each trajectory for 2^{22} time steps. The fluctuations observed in the tails of the PDF are attributed to finite-size effects, as only a finite number of initial conditions and time steps can be considered. These fluctuations diminish as N increases, provided the horizontal axis range is held fixed. Consequently, it is necessary to restrict the domain of the horizontal axis to an interval where the PDF does not exhibit highly fluctuating tails. To illustrate this, we display the PDF over a shorter interval in Fig. 3(b).

The PDFs of the variable X_j for several values of K are investigated in Ref. [5]. The authors selected positive values of K to account for the fact that the phase space contains a mixture of regular and chaotic trajectories, as also illustrated in Fig. 1 herein. They reported a consistent value of $q \approx 1.935$ (accurate to three decimal places) when fitting their numerical PDFs with Eq. (10) in cases corresponding to regular and weakly chaotic dynamics. In their study, the numerical PDF was found to take one of three forms: a Gaussian, a q-Gaussian, or a mixed-type distribution given by a linear combination of Gaussian and q-Gaussian PDFs.

In our analysis, we focus on reproducing the results presented in Ref. [5], specifically those shown in Figs. 4–5. To ensure consistency, we use the same number of trajectories and plot the corresponding PDFs using the parameters reported in their work.

The process of fitting the numerical PDF using Eq. (10) is described in the following section. We focus on cases where the numerical PDF is well approximated by a Gaussian distribution in the chaotic regime and by a q-Gaussian distribution in the regular and weakly chaotic regimes. We include the chaotic case here to demonstrate that our method can successfully compute the parameters q and b for the Gaussian distribution, thereby validating the approach before applying it to more challenging, non-Gaussian cases.

5. Fitting method

The parameters of the numerical PDF can vary significantly depending on the bin width used to compute them, as discussed in the previous section. This variation influences the values of q and b in Eq. (10). As a result, it is essential to select the best-fit PDF. Namely, the one that simultaneously satisfies the following criteria: (1) it must minimize the fitting error relative to the numerical PDF, and (2) it must integrate to an area as close as possible to 1. We define what we mean by "smallest error" when discussing the objective functions below.

Here we describe our approach to determine the parameters in Eq. (10) using a curve-fitting, multi-objective optimization method that enforces both criteria (1) and (2). Specifically, these two criteria form the basis of the two objective functions to be optimized simultaneously. For convenience, we rewrite the q-Gaussian PDF as

$$G_q(x) = a\left[1 - b(1-q)x^2\right]^{\frac{1}{1-q}}, \tag{10}$$

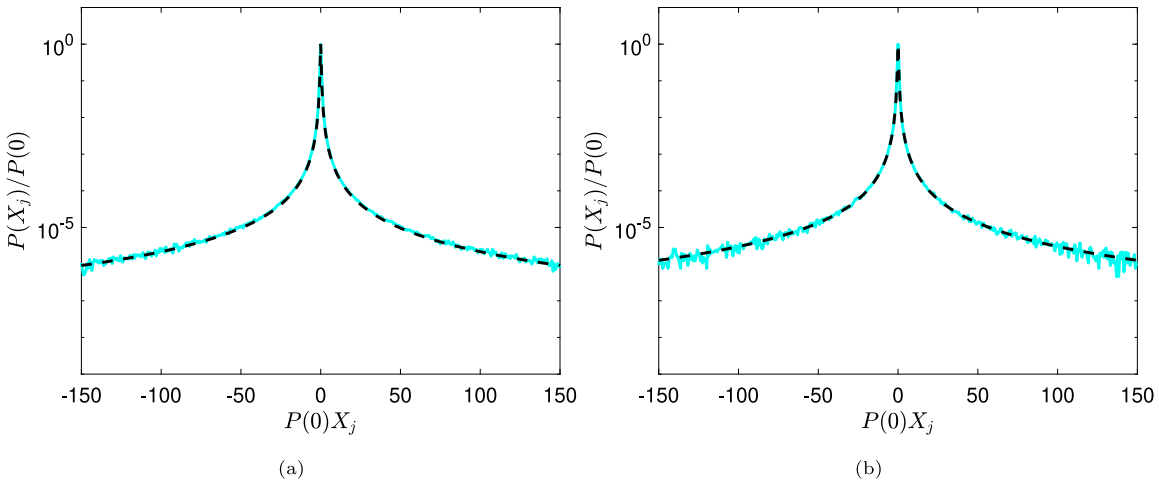

Fig. 4. Numerical PDF (blue curve) and corresponding q-Gaussian fit (black dashed curve) for $K = 0.2$ (panel (a)) and $K = 2$ (panel (b)), where the initial conditions are taken exclusively from a stability island. The number of initial conditions is 4×10^7 in panel (a) and 10^7 in panel (b), with the map iterated 2^{22} times in both cases. These PDFs are fitted using the q-Gaussian distribution given by Eq. (7), with parameter values $q = 1.935$ and $b_q = 21$ in panel (a), and $q = 1.935$ and $b_q = 15.5$ in panel (b).

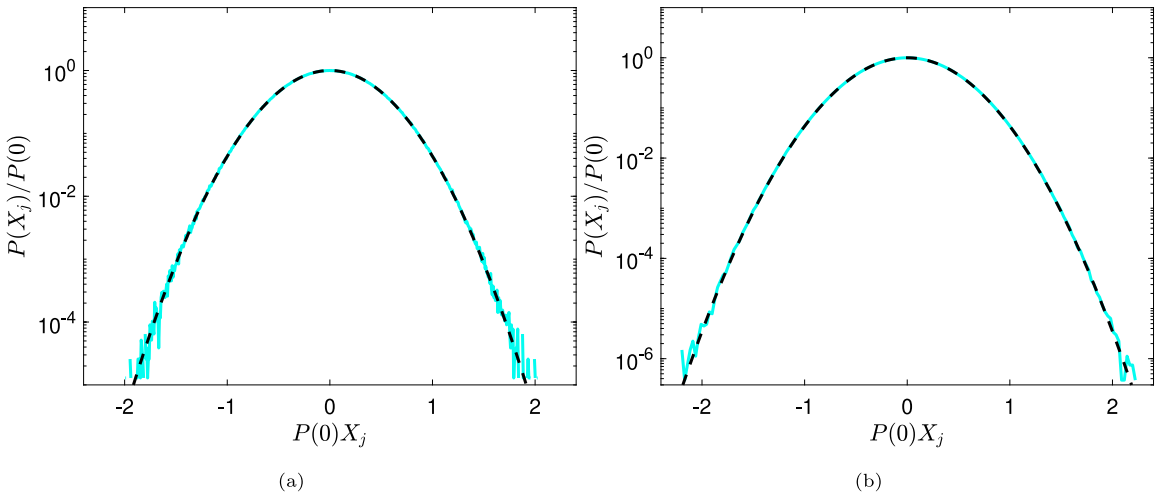

Fig. 5. Numerical PDF (blue curve) and corresponding q-Gaussian fit (black dashed curve) for $K = 10$ (panel (a)) and $K = 2$ (panel (b)), where the initial conditions are taken solely from the chaotic sea. In both cases, the number of initial conditions is 10^7, and the map is iterated for 2^{22} steps. These PDFs are fitted using the q-Gaussian distribution given by Eq. (7), with parameter values $q = 1$ and $b_q = 3.14$ in both panels, indicating that the distributions are Gaussian.

where a, b, and q are the model parameters. In particular, a is a normalization constant ensuring the total probability integrates to 1 over the domain of the distribution, b controls the width or spread, and q (the entropic index), governs the tail behavior of the distribution.

To quantify the quality of the fit, we define two objective functions: $f_1(x)$ corresponding to criterion (1) and $f_2(x)$ to criterion (2),

$$f_1(x) = \int_{\Omega(\epsilon)} \left| P(x) - G_q(x) \right| dx, \tag{11}$$

$$f_2(x) = \left| 1 - \int_{-\infty}^{\infty} G_q(x)\, dx \right|, \tag{12}$$

where

$$\Omega(\epsilon) = [-L, -L + \epsilon] \cup [L - \epsilon, L].$$

These functions encode the respective optimization goals: $f_1(x)$ measures the $\mathcal{L}_1$ distance between the numerical PDF $P(x)$ and the q-Gaussian fit $G_q(x)$, while $f_2(x)$ enforces proper normalization of the fitted PDF. Here, $2L$ denotes the total width of the interval under consideration, and ϵ specifies the tail region. When $\epsilon = L$, the domain becomes $\Omega(\epsilon) = [-L, L]$, and $f_1(x)$ reduces to the $\mathcal{L}_1$ norm over the full interval [21]. We use this norm as the error metric because it yields better results than alternative measures such as the sum of squared errors (SSE) or the root mean square error (RMSE).

When $0 < \epsilon < L$, especially for small ϵ, $f_1(x)$ captures the tail mismatch between $P(x)$ and $G_q(x)$. In our method, we solve the multi-objective optimization problem by starting with a small value of ϵ, thus initially fitting only the tails, and gradually increasing it until it covers the full domain ($\epsilon = L$).

Let

$$\Lambda = \left\{(x_i, y_i) : y_i = P(x_i), \text{ where } P \text{ is a numerical PDF of } X \text{ as in Eq. (9), across all bin widths } w\right\}.$$

We then formulate the multi-objective optimization problem as

$$\min\left\{f_1(x),\ f_2(x)\right\}, \tag{13}$$

subject to the constraints

$$P(x) \in \Lambda, \tag{14}$$

$$\epsilon \in [0, L]. \tag{15}$$

This optimization problem is solved using the procedure outlined in Algorithm 1 in Appendix. The algorithm is implemented via the `gamultiobj` solver, a built-in function in the Global Optimization Toolbox in MATLAB [22], which employs a genetic algorithm as described in [23]. The solver returns a Pareto front of non-dominated solutions, those that cannot be improved in one objective without worsening the other.

In this setting, an individual in the `gamultiobj` algorithm is defined as a vector (a, b, q) representing the parameters of the q-Gaussian distribution in Eq. (10). A population is a set of such individuals. The algorithm works as follows:

1. Selects parents for the next generation using binary tournament selection.
2. Generates offspring via Gaussian mutation and scattered crossover.
3. Evaluates the objective function values and feasibility of the offspring.
4. Merges the current and offspring populations into an extended population.
5. Computes the Pareto rank and crowding distance for all individuals.
6. Reduces the extended population back to the original population size by retaining top-ranked individuals.

We set the initial population size to 500. The initial parameter values are drawn uniformly from bounded intervals: a is sampled from a narrow interval around 1 to reflect normalization, $b > 0$, and $q \in [1, 3]$ [3]. The algorithm terminates when either the maximum number of generations (set to 10^4) is reached, or the function tolerance (set to 10^{-4}) is satisfied. Through experimentation, we found that this configuration balances numerical accuracy with computational efficiency.

In our experiments, we set $L = 150$ for regular cases and $L = 2$ for chaotic cases. The bin width is selected from the interval $[1, 150]$. A bin width smaller than 1 leads to excessive fluctuations, while one larger than 150 results in poor fit quality due to over-smoothing and loss of resolution.

6. Results

Here we discuss the results of the application of our proposed method in chaotic and regular cases of the standard map given in Eqs. (1), that is for $K = 0$, 0.2, 2 and 10. The chaotic case ($K = 10$) serves as the baseline of $q = 1$ of Gaussian PDFs, since the whole phase space is ergodic and the dynamics fully chaotic. This is to ensure our proposed method can find the theoretically predicted value of the q-entropic index in the chaotic case, that is $q = 1$. More interestingly, though, we want to check whether our approach yields indeed the same q entropic index (i.e., $q = 1.935$) in the case of regular and mixed regular and chaotic trajectories ($K = 0.2$ and 2), where the regular trajectories are more than the chaotic ones, as reported in [5]. Finally, we also consider the integrable case $K = 0$, for which the authors in [18] theoretically argue that $q = 2$, hence that the system is described by a q-Gaussian PDF. We want to see how close the numerical estimation of the q entropic index is to the theoretical value of $q = 2$, using our approach.

6.1. Chaotic case

We begin our analysis with the case of fully developed chaos, setting $K = 10$, where the numerical PDF is expected to closely follow the Gaussian distribution given in Eq. (4), characterized by $\widetilde{b} = \pi$. To verify this, we apply the fitting procedure described in Section 5, using Eq. (10) to approximate the numerical PDF generated according to the method outlined in Section 4. Specifically, we used 10^8 initial conditions, each iterated 2^{22} times.

The resulting parameters obtained through our optimization procedure are $b = 3.14208$ and $q = 1.00021$, both of which are very close to the theoretical Gaussian values $\widetilde{b} = \pi$ and $q = 1$. Fig. 6(a) displays the numerical PDF (turquoise curve) alongside the fitted q-Gaussian (black dashed curve), demonstrating strong agreement and providing compelling evidence that the distribution is indeed Gaussian.

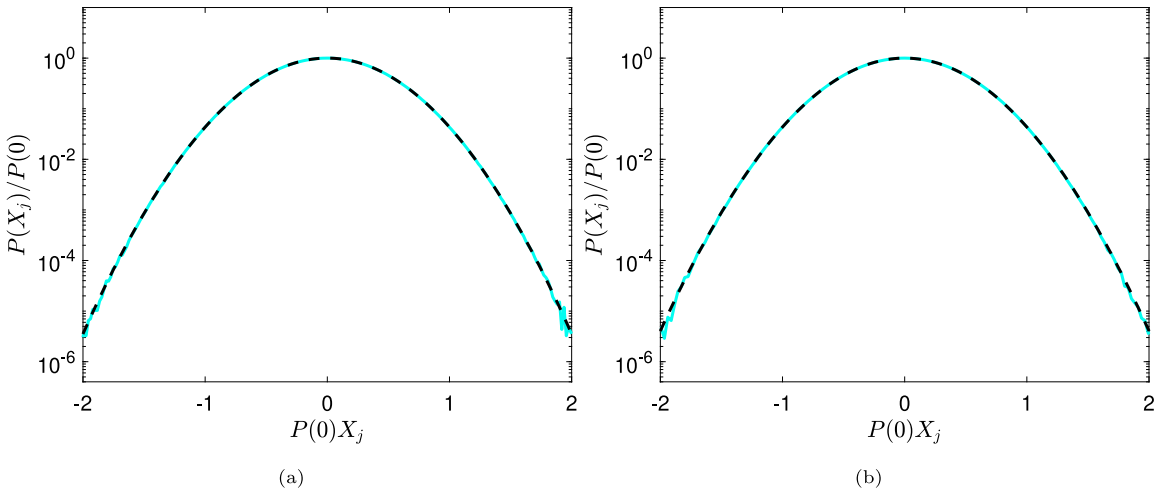

Fig. 6. The numerical PDF of the standard map (turquoise curve) and its corresponding q-Gaussian fit (black dashed curve) for $K = 10$ (panel (a)) and $K = 2$ (panel (b)). In both cases, the number of initial conditions is 10^8, and the map is iterated for 2^{22} steps. All initial conditions are chosen from the chaotic region. The fitted q-Gaussian parameters are $b = 3.14208$ and $q = 1.00021$ in panel (a), and $b = 3.14673$ and $q = 1.00218$ in panel (b).

The objective function values returned by our method are $f_1(x) = 8.0878 \times 10^{-4}$ and $f_2(x) = 7.0957 \times 10^{-9}$. Here, f_1 quantifies the $\mathcal{L}_1$ distance between the numerical PDF, $P(x)$, and the fitted q-Gaussian, $G_q(x)$, in Eq. (10), while f_2 measures the deviation of the total area under $P(x)$ from unity. The low values of both objective functions confirm the accuracy of the fit and the proper normalization of the PDF, validating the effectiveness of our method in recovering the theoretical parameters in a fully chaotic regime.

Next, we consider the case $K = 2$, selecting initial conditions from the chaotic sea (pale-yellow region in Fig. 2(c)). Applying the same methodology, the resulting fitted parameters are $b = 3.14673$ and $q = 1.00218$, again in close agreement with the Gaussian case. Fig. 6(b) shows the numerical PDF (turquoise) and its corresponding q-Gaussian fit (black dashed line), produced using the procedure described in Section 5. In this case, the objective functions are $f_1(x) = 1.20393 \times 10^{-3}$ and $f_2(x) = 8.83192 \times 10^{-7}$, which likewise indicate a strong match between the empirical and fitted PDFs. These findings reinforce the robustness of our approach and demonstrate its ability to retrieve accurate parameter values even in moderately chaotic regimes.

6.2. Regular case

Next, we examine the case $K = 0.2$, where most trajectories are regular and the chaotic regions are minimal. Figs. 1(a), obtained by iterating trajectories, and 2(a), derived by computing the maximal Lyapunov exponent over a grid of initial conditions, illustrate the phase space of the system, in which chaotic trajectories are barely visible. This corresponds to a non-chaotic regime, and we thus expect the PDFs to be described by q-Gaussians [5]. Using 10^8 initial conditions in the regular subdomain of the phase space (black region in Fig. 1(a)) and iterating for 2^{22} steps, the proposed method yields a q-Gaussian PDF with parameters $b = 8.10219$ and $q = 1.88153$, along with objective function values $f_1(x) = 5.74158 \times 10^{-2}$ and $f_2(x) = 1.11022 \times 10^{-15}$. These results indicate a good-quality fit between the numerical PDF and the q-Gaussian function given in Eq. (10), as also shown in Fig. 7(a). Notably, the q value reported here differs from that reported in [5], which may be attributed to differences in the fitting methodology. For instance, the earlier study may have employed a trial-and-error approach to fit the numerical PDFs, rather than a curve-fitting method based on least-squares minimization to reduce the residuals between the data points and the fitted curve.

Performing a similar analysis for $K = 2$, with initial conditions randomly chosen from the region of a stability island in Fig. 7(b), we obtain the q-Gaussian distribution parameters $b = 8.23001$ and $q = 1.89159$. The corresponding values of the optimized objective functions are $f_1(x) = 6.74877 \times 10^{-2}$ and $f_2(x) = 4.77706 \times 10^{-9}$, indicating a high-quality fit between the numerical PDF and the q-Gaussian function, as also illustrated in Fig. 7(b). In particular, the figure demonstrates a strong agreement between the numerical PDF (turquoise curve) and its fitted q-Gaussian distribution (black dashed curve). Again, the q value obtained here differs from the previously reported value $q = 1.935$ in [5], a discrepancy that may arise for the same reasons discussed earlier in the context of our results for $K = 0.2$.

Next, we consider the case $K = 0$, for which the standard map (1) becomes integrable. In this regime, the phase space (x, p) contains no chaotic trajectories, and all orbits evolve along straight lines with constant slope, wrapping periodically due to the modulo operation, as illustrated in Fig. 8. Bountis et al. [18] reported that the dynamics in this case follow a q-Gaussian distribution (10) with $q = 2$. This differs from the value $q = 1.935$ obtained by Tirnakli et al. [5] for regular trajectories at $K = 0.2$ and $K = 2$, as well as from our own estimates of $q = 1.88153$ and $q = 1.89159$ for these respective values of K. Therefore, our next

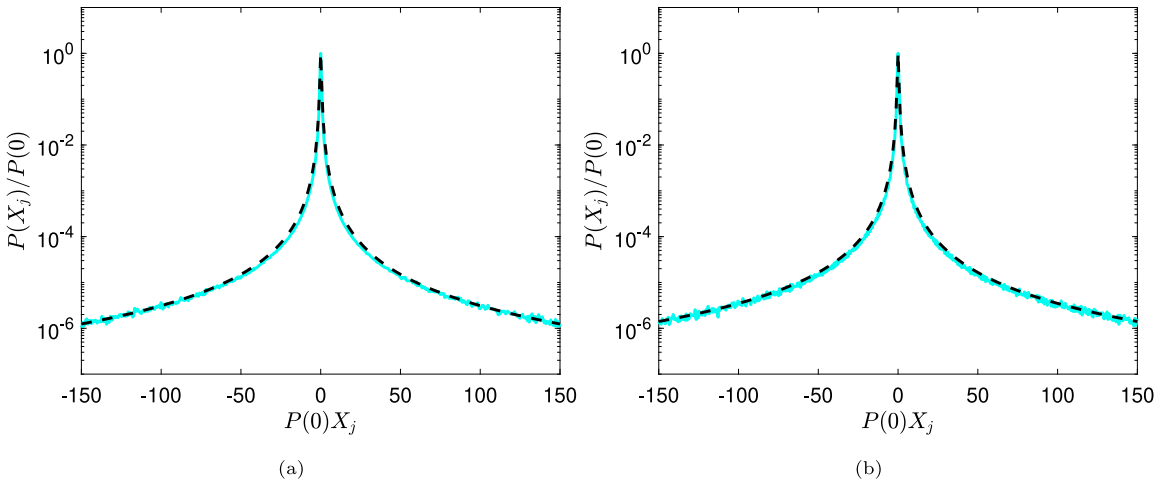

Fig. 7. The numerical PDF of the standard map (turquoise curve) and its corresponding q-Gaussian function (black dashed curve) are shown for $K = 0.2$ (panel (a)) and $K = 2$ (panel (b)). In both cases, the number of initial conditions is 10^8, and the map is iterated for 2^{22} times. All initial conditions are chosen from a stable region of the standard map. The fitted q-Gaussian distribution parameters are $b = 8.10219$ and $q = 1.88153$ in panel (a), and $b = 8.23001$ and $q = 1.89159$ in panel (b).

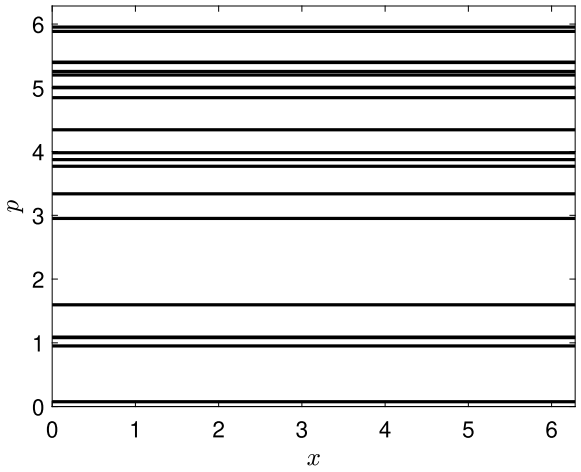

Fig. 8. Phase portrait (x, p) of the standard map for the integrable case $K = 0$.

objective is to investigate whether our methodology applied to the integrable case $K = 0$ can produce a q value approaching 2, as reported in [18], and, in particular, to estimate the number of iterations required for q to converge to this value.

In particular, Bountis et al. [18] reported that for $K = 0$, their parameters were $a = 4$, $b = 16\pi^2$, and $q = 2$, using the (non-normalized) q-Gaussian function (10). In contrast, here we adopt the normalized form of the q-Gaussian given in Eq. (7), which, following the derivations in Section 3, corresponds to $a = 1$, $b = \pi^2$, and $q = 2$.

Next, we perform two computational studies to assess the convergence of the fitted PDF parameters toward these theoretical values as the number of initial conditions increases. Specifically, we consider $M = 10^8$ and $M = 10^9$ initial conditions, each iterated 2^{22} times, to investigate how increasing M affects the resulting PDF and its fitting parameters. In the first study with $M = 10^8$, our method yields $b = 8.42148$ and $q = 1.90619$, with objective function values $f_1(x) = 6.14898 \times 10^{-2}$ and $f_2(x) = 3.64456 \times 10^{-8}$. In the second study with $M = 10^9$, the corresponding results are $b = 8.46807$ and $q = 1.90966$, with $f_1(x) = 5.56503 \times 10^{-2}$ and $f_2(x) = 5.67387 \times 10^{-7}$. Despite increasing the number of initial conditions by one order of magnitude, the computed values of b and q remain noticeably different from the normalized theoretical values $b = \pi^2 \approx 9.8696044$ and $q = 2$ derived from [18]. Fig. 10 illustrates the numerical PDFs from both studies: panel (a) displays the result for $M = 10^8$ initial conditions, and panel (b) for $M = 10^9$, with the numerical PDF shown in turquoise and its best-fit q-Gaussian in black dashed curves.

Based on these results, we conclude that increasing the number of trajectories by an order of magnitude does not significantly affect the shape of the resulting PDF, as the fitted values of b and q remain nearly identical in both cases. Moreover, our estimated q values remain below 2, deviating from the result reported in [18]. These findings suggest that achieving a numerically accurate

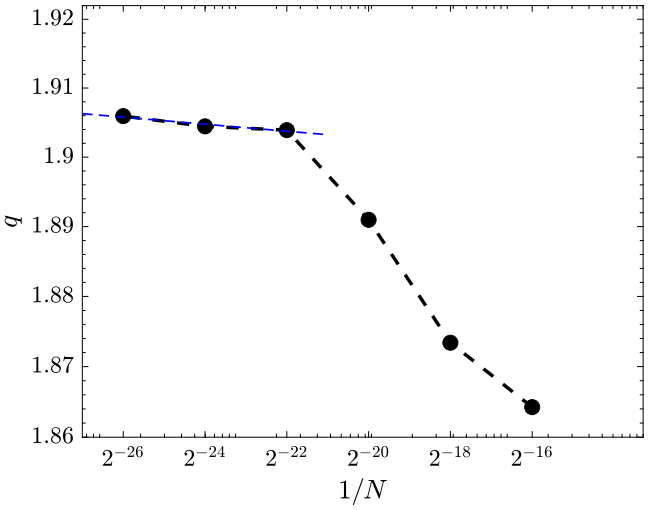

Fig. 9. Estimated q values as a function of $1/N$ for the integrable case $K = 0$ with 10^7 initial conditions. The plot shows that as $1/N \to 0$, the estimated q approaches the theoretical value $q = 2$, illustrating the asymptotic behavior of the method. The blue curve represents the fitted power-law function applied to the three largest N values, capturing the slow convergence toward the theoretical limit.

PDF characterized by $q = 2$ may require an extremely large ensemble of trajectories, potentially exceeding 10^9, and possibly longer iteration times than 2^{22}. Furthermore, our results reveal only a marginal increase in q as the number of trajectories grows, indicating that convergence toward $q = 2$ is likely a very slow process, necessitating a vast number of iterations.

This motivated us to further investigate the asymptotic behavior of the estimated q in the integrable case ($K = 0$). We fixed the number of initial conditions to 10^7 and varied the number of iterations as $N = 2^{16}, 2^{18}, 2^{20}, 2^{22}, 2^{24}, 2^{26}$. Applying our method to each case yielded q values of 1.86425, 1.87340, 1.89098, 1.90390, 1.90445, and 1.90593, respectively. These results reveal a clear trend: as N increases (or equivalently, as $1/N \to 0$), the estimated q gradually approaches the theoretical value $q = 2$. Fig. 9 illustrates this asymptotic tendency by plotting q as a function of $1/N$.

To further investigate the convergence behavior illustrated in Fig. 9, we analyzed the data using a power-law model $y(x) = a\,x^b$, which effectively characterizes scaling relations that appear linear on a log–log scale. The results reveal two distinct regimes: for smaller iteration counts ($N = 2^{16}$ to 2^{22}), the estimated q increases relatively rapidly, whereas for larger values ($N = 2^{22}$ to 2^{26}), the variation becomes slower and nearly linear in the log–log representation, suggesting an asymptotic scaling behavior. A power-law fit applied to the three largest N values yields $a \approx 1.89$ and $b \approx -3.8 \times 10^{-4}$, indicating an exceptionally slow approach toward the theoretical limit. The fitted curve is shown in blue in Fig. 9. Extrapolating this fit suggests that approximately $2^{51} \approx 2.25 \times 10^{15}$ iterations would be required for the estimated q to effectively attain its theoretical value of $q = 2$, something that cannot be achieved with current computational capabilities.

7. Conclusions

In this study, we analyzed the probability density functions (PDFs) derived from the dynamics of the standard map across chaotic, regular, and integrable regimes. Our central goal was to develop a systematic and reliable framework for estimating the parameters of the q-Gaussian distribution, a cornerstone of non-extensive statistical mechanics for describing systems that deviate from the Boltzmann–Gibbs paradigm.

To achieve this, we formulated parameter estimation as a *multi-objective optimization problem* and employed a *genetic algorithm* to concurrently (i) minimize the discrepancy between the numerical PDF and the fitted q-Gaussian, and (ii) ensure proper normalization of the fitted distribution. This dual-objective framework allowed for a comprehensive exploration of the parameter space, yielding optimal values of q and b that closely matched the numerically computed PDFs across different dynamical regimes of the standard map.

The use of a genetic algorithm enabled a population-based search guided by the objective functions defined in Eqs. (11) and (12), thereby ensuring both statistical accuracy and normalization consistency. In contrast to previous studies such as [16], which relied primarily on heuristic or single-objective fitting procedures, our approach provides a principled and reproducible means of parameter inference. The slight deviations in our estimated q values relative to earlier works can likely be attributed to this methodological refinement and to our explicit enforcement of normalization during optimization.

In the *integrable case* ($K = 0$), we further examined the asymptotic behavior of the estimated q by varying both the number of trajectories and iteration length. Increasing the number of trajectories by an order of magnitude produced negligible changes in the fitted parameters, suggesting convergence in the PDF shape. However, the estimated q values remained below the theoretical prediction $q = 2$ reported in [18]. Our detailed scaling analysis, modeled using a power-law relation, revealed that q approaches

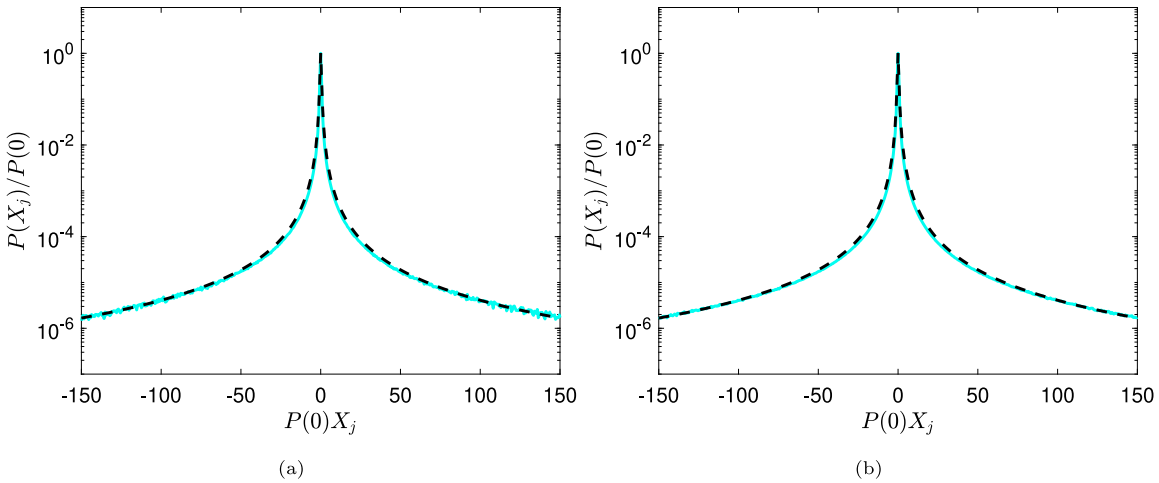

Fig. 10. The numerical PDF of the standard map (turquoise curve) and its corresponding q-Gaussian function (black dashed curve) for $K = 0$, shown for (a) $M = 10^8$ initial conditions and (b) $M = 10^9$ initial conditions. In both cases, the map is iterated for 2^{22} steps. The fitted parameters of the q-Gaussian distribution are $b = 8.42148$ and $q = 1.90619$ in panel (a), and $b = 8.46807$ and $q = 1.90966$ in panel (b).

2 extremely slowly with increasing iteration number, following an asymptotic trend consistent with Fig. 9. The fitted power-law $y(x) = a\,x^b$ with $a \approx 1.89$ and $b \approx -3.8 \times 10^{-4}$ implies that approximately $2^{51} \approx 2.25 \times 10^{15}$ iterations would be required for q to effectively reach 2, underscoring the exceptionally slow convergence of the distribution toward its theoretical limit.

Overall, our results demonstrate that the proposed multi-objective optimization framework provides a robust and generalizable methodology for quantifying the statistical properties of deterministic dynamical systems. Its success in reproducing q-Gaussian behavior across chaotic, regular, and integrable regimes highlights its versatility and potential applicability to a broader class of maps and continuous-time systems. We anticipate that future extensions of this approach could help elucidate universal features of non-extensive statistics and their emergence in complex dynamical processes.

CRediT authorship contribution statement

Zulkarnain: Writing – review & editing, Writing – original draft, Validation, Software, Formal analysis. **H. Susanto:** Writing – review & editing, Validation, Supervision. **C.G. Antonopoulos:** Writing – review & editing, Writing – original draft, Validation, Supervision, Methodology, Conceptualization.

Declaration of Generative AI and AI-assisted technologies in the writing process

During the preparation of this work, the authors used Grammarly and ChatGPT in order to improve language and readability. After using these tools/services, the authors reviewed and edited the content as needed and took full responsibility for the content of the publication.

Declaration of competing interest

The authors declare that they have no known competing financial interests or personal relationships that could have appeared to influence the work reported in this paper.

Acknowledgments

Z is supported by the Ministry of Education, Culture, Research, and Technology of Indonesia through a PhD scholarship (BPPLN). HS acknowledges support by Khalifa University through a Competitive Internal Research Awards Grant (No. 8474000413/CIRA-2021-065) and Research & Innovation Grants (No. 8474000617/RIG-S-2023-031 and No. 8474000789/RIG-S-2024-070). Portions of this work were previously included in Z's doctoral thesis, submitted to the University of Essex in 2024. The authors acknowledge the use of the High Performance Computing Facility (Ceres) and its associated support services at the University of Essex in the completion of this work.

Appendix

This appendix presents the detailed algorithm used in the numerical simulations described in this study. It is provided here for completeness and to facilitate reproducibility of the results.

Algorithm 1 q-Gaussian probability density function (PDF) optimization procedure

Require: Variables X_j as given in Eq. (9), length of the fitting interval L, bin width minimum $w_{\min}$, bin width maximum $w_{\max}$.
Ensure: q-Gaussian distribution parameters (a, b, q), objective function values $f_1(x)$ and $f_2(x)$.

$S \leftarrow \emptyset$
for $\epsilon = 0$ to L **do**
  for $w = w_{\min}$ to $w_{\max}$ **do**
    Generate numerical PDF with bin width w.
    Solve Eq. (13) subject to (14)–(15) using genetic algorithm multi-objective solver.
    Store all solutions (a, b, q) in $\mathcal{N}$.
  end for
  for $k = 1$ to length($\mathcal{N}$) **do**
    $f_1^L(x) \leftarrow f_1(x)$ for $x \in \Omega(L)$, using parameters $\mathcal{N}(k)$
    $\mathcal{P}(k) \leftarrow f_1^L(x) + f_2(x)$, using parameters $\mathcal{N}(k)$.
  end for
  Compute $\min\{\mathcal{P}\}$. Store the corresponding set of parameter from $\mathcal{N}$ to S.
end for
for $k = 1$ to length(S) **do**
  for $\epsilon = 0$ to L **do**
    $f_1^{\text{opt}}(x) \leftarrow f_1(x)$ for $x \in \Omega(\epsilon)$, using parameters $S(k)$
    $\mathcal{P}^{opt}(k) \leftarrow f_1^{\text{opt}}(x)$, using parameters $S(k)$.
  end for
end for
Compute $\min\{\mathcal{P}^{opt}\}$. Report the corresponding set of parameters from S as the optimum solution S^{opt}.
Compute $f_1(x)$ and $f_2(x)$ using the set of parameters in S^{opt}.

Data availability

The data that support the findings of this study are available within the article.

References

[1] Chirikov BV. A universal instability of many-dimensional oscillator systems. Phys Rep 1979;52(5):263–379.
[2] Lichtenberg AJ, Lieberman MA. Regular and chaotic dynamics. Springer-Verlag; 1992.
[3] Tsallis C. Introduction to nonextensive statistical mechanics: Approaching a complex world. Springer; 2009.
[4] Ruiz G, Tirnakli U, Borges EP, Tsallis C. Statistical characterization of the standard map. J Stat Mech Theory Exp 2017;2017(6):aa728b.
[5] Tirnakli U, Borges EP. The standard map: From Boltzmann-Gibbs statistics to Tsallis statistics. Sci Rep 2016;6:2–9.
[6] Tsallis C. Possible generalization of Boltzmann-Gibbs statistics. J Stat Phys 1988;52(1–2):479–87.
[7] Antonopoulos CG, Bountis T, Skokos C, Drossos L. Complex statistics and diffusion in nonlinear disordered particle chains. Chaos: An Interdiscip J Nonlinear Sci 2014;24(2).
[8] Antonopoulos CG, Skokos C, Bountis T, Flach S. Analyzing chaos in higher order disordered quartic-sextic Klein-Gordon lattices using q-statistics. Chaos Solitons Fractals 2017;104:129–34.
[9] Antonopoulos CG, Bountis T, Drossos L. Coupled symplectic maps as models for subdiffusive processes in disordered Hamiltonian lattices. Appl Numer Math 2016;104:110–9.
[10] Antonopoulos CG, Christodoulidi H. Weak chaos detection in the Fermi–Pasta–Ulam-α system using q-Gaussian statistics. Int J Bifurc Chaos 2011;21(08):2285–96.
[11] Antonopoulos C, Bountis T, Basios V. Quasi-stationary chaotic states in multi-dimensional Hamiltonian systems. Phys A 2011;390(20):3290–307.
[12] Chirikov BV. Research concerning the theory of non-linear resonance and stochasticity. Geneva: CERN; 1971, Translated at CERN from the Russian (IYAF-267-TRANS-E).
[13] Chirikov BV. A universal instability of many-dimensional oscillator systems. Phys Rep 1979;52(5):263–379.
[14] Zaslavsky GM. Hamiltonian dynamics. In: Hamiltonian chaos and fractional dynamics. Oxford University Press; 2004.
[15] Ott E. Chaos in dynamical systems. Cambridge University Press New York; 2002.
[16] Tirnakli U, Tsallis C. Extensive numerical results for integrable case of standard map. Nonlinear Phenom Complex Syst 2020;23(2):149–52.
[17] Benettin G, Galgani L, Giorgilli A, Strelcyn J-M. Lyapunov characteristic exponents for smooth dynamical systems and for Hamiltonian systems; a method for computing all of them. Part 1: Theory. Meccanica 1980;15(1):9–20.
[18] Bountis A, Veerman JJP, Vivaldi F. Cauchy distributions for the integrable standard map. Phys Lett A 2020;384(26):126659.
[19] Robledo A. Criticality in nonlinear dynamics: The route to nonextensive statistical mechanics. Phys A 2002;314(1–4):437–44.
[20] Mitchell M. An introduction to genetic algorithms. MIT Press; 1998.
[21] Stein EM, Shakarchi R. In: Functional analysis: introduction to further topics in analysis, vol. 4, Princeton University Press; 2011.
[22] The MathWorks Inc. gamultiobj Algorithm. Natick, Massachusetts, United States: The MathWorks Inc.; 2023, https://uk.mathworks.com/help/gads/gamultiobj-algorithm.html.
[23] Deb K. Multi-objective optimisation using evolutionary algorithms: an introduction. In: Multi-objective evolutionary optimisation for product design and manufacturing. Springer; 2011, p. 3–34.